1K2-IOS-1b-3

Spatio-temporal Kriging of solar radiation incorporating direction and speed of cloud movement

Tsuyoshi Inoue[*1] Tetsuo Sasaki[*2] Takashi Washio[*3]

[*1] Mitsubishi Research Institute, Inc. [*2] The Kansai Electric Power Co., Inc. [*3]Osaka University

The spatial distribution of solar radiation, corresponding to a cloud pattern, moves according to winds aloft and changes shape. This report analyzes distributed observations of solar radiation to identify statistical characteristics of the motion. 25 observations around Osaka area are used to analyze spatial correlation patterns with delay, and the results are compared to whole-sky photographs. The correlation patterns differ according to cloud pattern and motion, yet when the motion of cloud is observed, the speed and direction of the cloud motion can be identified from the correlation pattern. Using the information above, a detailed map of solar radiation (spatial and temporal resolution of 500 meters and 5 minutes) could be drawn by spatio-temporal Kriging. The presented method parameterizes the direction and speed of a cloud cover ratio, thereby incorporating its directionality. Cross-validation with spatial Kriging shows the advantage of spatio-temporal Kriging when the motion of cloud is observed.

1. Introduction

Large-scale penetration of PV, in terms of both climate change mitigation and energy diversity, is expected in the near future. In order to properly understand its implications and prepare for it, it is necessary to quantify solar output volume and variability. This is leading to the needs for solar radiation information with different level of spatial and temporal resolution. While observations at meteorological stations or by satellite imagery have long existed, information with higher resolution is becoming necessary.

This report uses solar radiation data taken from 25 observation stations around Osaka. Distances between stations are around 3-4.5km, and the temporal resolution is 1 second. The data is used to analyze spatio-temporal correlation pattern of solar radiation. The correlation pattern, calculated from observation, is then modeled by a theoretical covariance function. Then it is used for spatio-temporal Kriging to get gridded datasets with spatial resolution 500m, temporal resolution 5min, for Osaka area. The overall procedure is summarized in Figure 1.

Difference with existing solar variability study is the emphasis on the motion of the spatial pattern of radiation, mainly generated by cloud formation, motion and dissolution. Ordinarily, variability of the output is expressed as a function of distance and time-scale (for example in [Lave 2011]). When two locations are further apart, they are less strongly correlated. In this report, correlation is examined in two dimensions and with temporal delay. This allows us to express solar variability as clusters moving in particular direction. This kind of analysis, and the obtained map of solar radiation, could lead to better understanding of solar variation.

2. Analysis

2.1 Correlation pattern of solar radiation

April 21, 2011 is selected for the analysis. A sunny day with thin cloud is selected so as to include relatively large variability of radiation (Figure 2). For the analysis, observed global solar irradiance is converted to clearness index, which is a normalized radiation relative to theoretical radiation at the top of the atmosphere. The original data has temporal resolution of 1 second. It is averaged across 5 minutes in order to cut off changes with high frequency, which is related to small-scale change of cloud pattern.

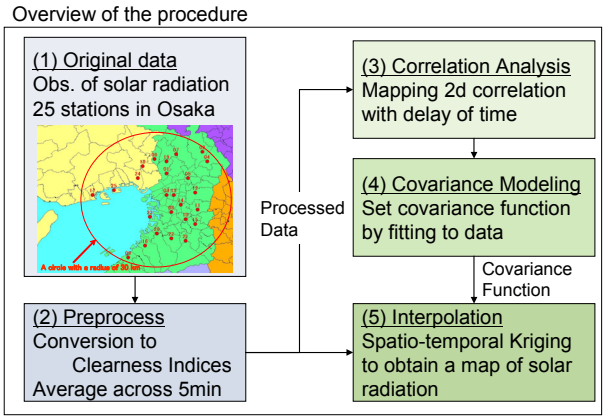

Figure 1: Overview of the analytical procedure.

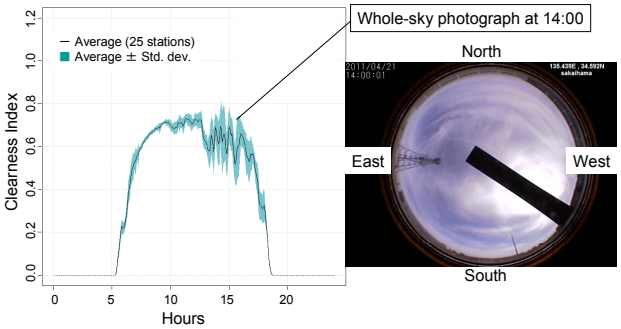

Figure 2: Basic characteristics of the selected day. Left: time series of averaged clearness index. Right: a whole-sky photograph taken at 14:00.

Contact: Tsuyoshi Inoue, Mitsubishi Research Institute, Inc., 10-3, Nagatacho 2-Chome, Chiyoda-Ku, Tokyo 100-8141, Phone: 03-6705-5568, E-mail: tsuyoshi@mri.co.jp

Figure 3 shows covariance pattern of the day. For every pair of observation points, magnitude of covariance is plotted at position relative to each other. Hence there are 25 observation stations, the total of 25^2=625 points are plotted. Four maps correspond to the covariance plot with delays of 0, 5, 10, 15 minutes. This three-dimensional view of the covariance allows us to identify a clear pattern which is moving in one direction while getting weaker with the passage of time. This pattern cannot be viewed if only one-dimensional distance is used.

Comparison with higher altitude wind observation at Shionomisaki (140km south from Osaka) shows that the direction and speed of the motion corresponds to wind direction and speed of higher altitude (altitude 8-10km, wind velocity 31-35m/s, wind direction northwest in this case). Whole-sky photographs taken at Sakaihama (around center of the study area) show that the moving direction of the covariance pattern corresponds to direction of cloud movement. Cloud type can be interpreted as cirrus (Ci), which is a type of high-altitude cloud. Those evidences suggest that the correlation pattern by cloud movement can be captured by spatially distributed observations of solar radiation.

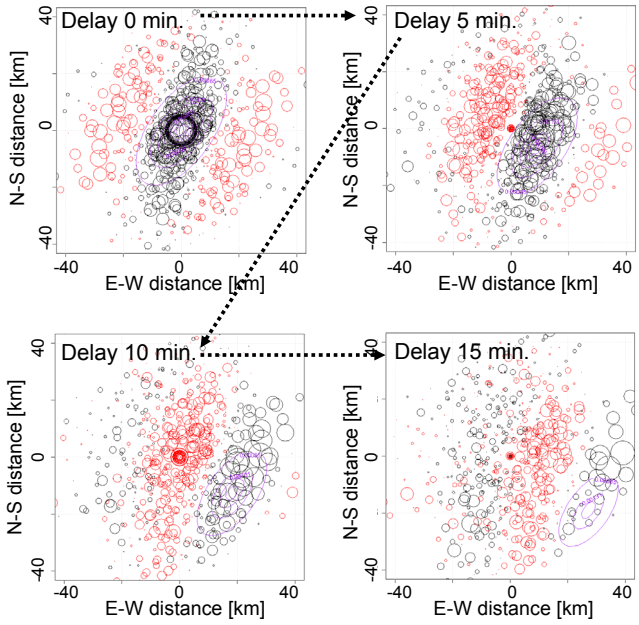

Figure 3: Plot of covariance pattern with delay of time. Black (red) points are positively (negatively) correlated. Purple contours denote the modeled covariance function (see 2.2 for details).

2.2 Spatio-temporal Kriging

The covariance pattern above can be utilized to obtain a spatial distribution of solar radiation. We use spatio-temporal Kriging, which can account for the observed covariance pattern. Spatio-temporal Kriging is an extension of spatial Kriging so that the past data can also be used. The value Z* at a position x_0 and time t_0 is estimated by a weighted average of observations at positions x_i, t_i.

$$Z^*(\mathbf{x}_0, t_0) = \sum_{i=1}^{n} w_i Z(\mathbf{x}_i, t_i)$$

The weighs w_i are determined so as to minimize variance of estimated value. As a result, the weights are calculated by solving the linear equation below (for a detailed formulation, see [Cressie & Wilke 2011] for example).

$$\sum_{j=1}^{n} w_j \gamma(\mathbf{x}_i - \mathbf{x}_j, t_i - t_j) + \mu = \gamma(\mathbf{x}_i - \mathbf{x}_0, t_i - t_0) \qquad (i = 1,..,n)$$

$$\sum_{j=1}^{n} w_j = 1$$

Where $\gamma(\mathbf{h}, \tau)$ is the variogram, which is assumed to be solely determined by the difference of location and time. When the variance of Z is finite, the variogram can be expressed with covariance function (covariogram) $C(\mathbf{h}, \tau)$ as follows.

$$\gamma(\mathbf{h}, \tau) = C(\mathbf{0}, 0) - C(\mathbf{h}, \tau)$$

The covariance function is selected so that it can explain observed pattern of covariance, and several types of basic functions are available. In this study we set the covariance function as follows.

$$C(\mathbf{h}, \tau) = \sigma^2 \exp[-((\mathbf{h} - \boldsymbol{v}\tau)^T \Sigma (\mathbf{h} - \boldsymbol{v}\tau))^{1/2} - c\tau],$$

$$\Sigma = diag(a^2, b^2), \qquad \mathbf{h}' = R(\varphi)\mathbf{h}$$

Figure 4 is a schematic diagram of the function. Basically, the covariance is diminishing exponentially in both distance and time. With the "motion vector" parameter $\mathbf{v}=(v_x, v_y)$, the center of the covariance moves in one direction. Because of this, the covariance function is non-separable and asymmetric. This type of covariance function is sometimes called to satisfy Taylor's hypothesis [Sherman 2011].

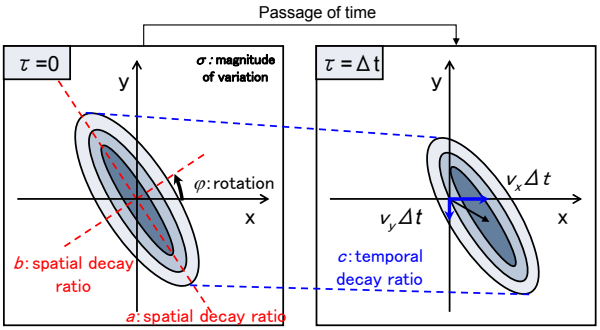

Figure 4: Setting of covariance function.

The parameters are estimated from the covariance data of Figure 3. The estimated function is superimposed on the plot of covariance. The estimation is sequentially done for $\mathbf{v}$, σ, a, b, and then c in the following manner.

(1) Motion vector $\mathbf{v}$:
Temporal delay for an arbitrary pair of clearness index observations is calculated by taking the maximum of cross-correlation. Using relative positions and corresponding temporal delay, the motion vector is estimated.

(2) Overall standard deviation σ :
The mean of the standard deviations for each observation station is used.

(3) Spatial decay coefficients a,b :
Covariance data with no delay is used to estimate a and b. The linear least-square method is applied to log-transformed data.

(4) Temporal decay coefficient c :
Incorporating all the parameters above, c can be estimated by the linear least-square method with log transformation.

The estimated parameters for the selected day are shown in Table 1.

Table 1: Selected parameters of covariance function.

Vx [m/s]	Vy [m/s]	ϕ [rad]	σ^2	a	b	c
36.4	-8.0	1.74	0.006	0.201	0.099	0.050

3. Results

3.1 Characteristics of spatio-temporal Kriging

The above method is applied to calculate maps of the clearness index at April 21, 2011. Figure 5 shows the comparison with the maps produced by spatial Kriging (spherical variogram is used). Maps by spatio-temporal Kriging show smooth transition of cloudy areas (denoted in red circles), whereas those by spatial Kriging are disconnected.

Cross-validation by leave-one-out method is used to quantitatively compare the error by the two methods. Figure 6 shows the time series for RMSE of the cross-validation. Spatio-temporal Kriging is effective in the afternoon, when the variation gets wild. Daily averaged RMSE of spatio-temporal Kriging is 0.039, whereas that of spatial Kriging is 0.045. A small improvement is confirmed.

3.2 Remarks on spatial and temporal scale

Current settings of spatial resolution 500m and temporal resolution 5min are determined by the configuration of the observation stations. If observation points are more densely situated, higher spatial-temporal resolution can be achieved. When the distance between locations gets closer, correlation starts to appear even in shorter timescales.

We have also obtained observations at the large-scale photovoltaic power plant in Sakai, which has 12 measurements in the rectangular area of 400m x 800m. Analysis of the data shows that, at that resolution, temporal resolution of 30sec is practical. This shows that the same analytical procedure could be used for different spatial scales.

This method assumes that covariance characteristics remain the same during the day. This is generally incorrect, since weather could change anytime during a day. By dividing the analysis period into segments with similar characteristics, the result could be further improved. However, each segment should be long enough for calculating covariance between time series (when the temporal resolution is 5 minutes, at least 1-2 hours of observation is necessary).

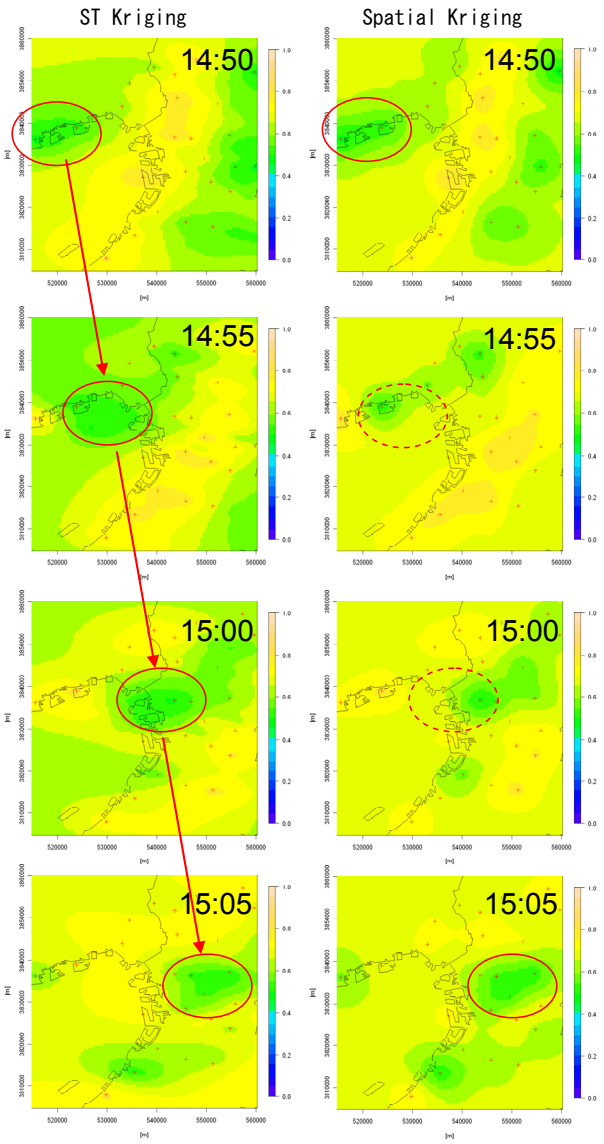

Figure 5: Map of clearness indices generated by spatio-temporal Kriging(left) and spatial Kriging(right). Locations of observational stations are denoted by red plus signs.

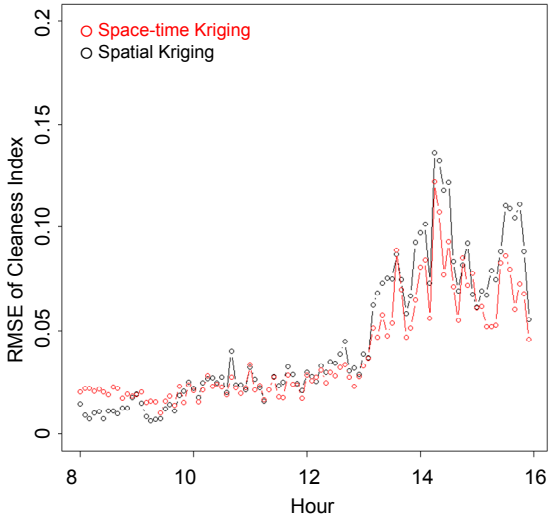

Figure 6: Time series of RMSE by a cross-validation.

3.3 Dependence of applicability on weather

The above analytical procedure is strongly dependent on weather conditions. Analysis on different day creates covariance patterns of different characteristics. Figure 7 shows the analyses on April 20 and 22. The sky of April 20 has rows of small clouds, and the reflection and refraction on the cloud is large. Because of its randomness, no distinct pattern can be detected from the covariance plot. April 22 is an overcast day with consistent motion of the cloud. An oval pattern is found, and when plotted with time delay, the motion of the pattern is observed (note that the oval direction of the pattern is different from that of April 21).

In order to confirm the overall applicability of the above method, one-year observational record (from December 2010 to November 2011) is analyzed. Presence of the covariance pattern and its motion are examined visually. As a result, on about a third of the days (110 days), clear covariance patterns are confirmed. This suggests the applicability of spatio-temporal Kriging for these days. However, a quantitative judgment of error (for example by cross-validation) is still needed to properly evaluate the effectiveness of spatio-temporal Kriging.

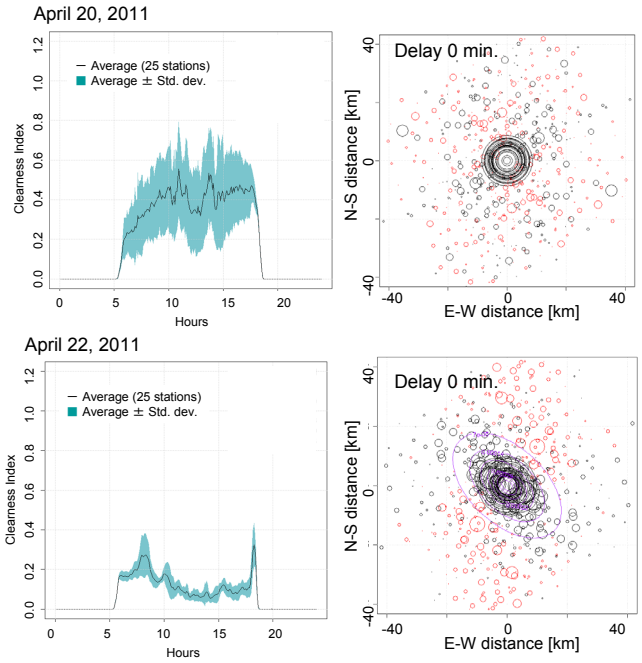

Figure 7: Dependence of covariance on radiation pattern. (Example on April 20 and April 22, 2011.)

4. Conclusion

In this report we have shown the applicability of a spatio-temporal statistical analysis to geographically distributed solar radiation data. Covariance analysis is used to explain the movement of the solar radiation generated by the cloud. Using the result, spatio-temporal Kriging is applied to obtain distributions of the solar radiation. The result is favorable, in terms of both estimation error and visual characteristics.

The procedure presented above can be used to generate a detailed dataset of solar radiation distribution (with spatial resolution 500m and temporal resolution 5min.) Using the dataset, we plan to continue the analysis of solar variability based on the understanding of this study.

5. Acknowledgements

We thank members of “Project for Stabilization of Electric Power System and Promotion for High Penetration of Distributed New-energy” supported by the Japanese Agency for Natural Resources and Energy for the collection of observational data.

References

[Lave 2011] Matthew Lave, Jan Kleissl, Ery Arias-Castro, High-frequency irradiance fluctuations and geographic smoothing, Solar Energy, In Press, Available online 31 August 2011.

[Cressie & Wilke 2011] Noel Cressie and Christopher K. Wilke, Statistics for Spatio-Temporal Data, Wiley, 2011.

[Sherman 2011] Michael Sherman, Spatial Statistics and Spatio-Temporal Data, Wiley, 2011.